RSC Advances

PAPER

View Article Online
View Journal | View Issue

Cite this: *RSC Adv.*, 2016, **6**, 100145

Non-stoichiometric Cu–In–S@ZnS nanoparticles produced in aqueous solutions as light harvesters for liquid-junction photoelectrochemical solar cells†

Alexandra Raevskaya,[a] Oksana Rosovik,[a] Andriy Kozytskiy,[a] Oleksandr Stroyuk,*[a] Volodymyr Dzhagan[bc] and Dietrich R. T. Zahn[c]

A direct "green" aqueous synthesis of mercapto acetate-stabilized copper indium sulfide (CIS) nanoparticles (NPs) and core/shell CIS@ZnS NPs of a varied composition under ambient conditions and a temperature lower than 100 °C is reported. The CIS@ZnS NPs can be anchored to the surface of nanocrystalline FTO/TiO_2 films without additional purification or ligand exchange steps yielding visible-light-sensitive heterostructures ready for using as photoanodes in the liquid-junction solar cells. The highest photoelectrochemical activity in a three-electrode cell was demonstrated by a TiO_2/CIS@ZnS heterostructure with atomic Cu : In : S and Zn : Cu ratios of 1 : 5 : 10 and 1 : 1. The optimized TiO_2/CIS@ZnS photoanodes were tested in two-electrode solar cells with aqueous polysulfide electrolyte and TiO_2/Cu_2S heterostructures produced by a photo-assisted method as counter-electrodes. Under illumination by a 30 mW cm^{-2} xenon lamp, the optimized cells showed the average light conversion efficiency of 8.15%, the average open-circuit voltage of −0.6 V and the average fill factor of 0.42. The cells revealed excellent stability and reproducibility of photoelectrochemical parameters with around one percent variation of the light conversion efficiency around an average value for six identical solar cells.

Received 18th July 2016
Accepted 14th October 2016

DOI: 10.1039/c6ra18313a

www.rsc.org/advances

Introduction

The nanoparticles (NPs) of cadmium and lead chalcogenide semiconductors combine strong absorbance in the UV/visible spectral range, prominent luminescent and/or photochemical properties, and pronounced size dependences of the photophysical characteristics due to confinement effects. The favorable combination of the properties has attracted to these compounds immense attention resulting in a variety of applications, in particular, in the photovoltaics and photocatalysis, the light-emitting diode technologies, the luminescent biosensors, and bio-analysis, *etc.*[1–4] However, the cadmium and lead chalcogenide NPs are inherently toxic and, therefore, a considerable effort has been currently applied to reveal alternative luminescent and/or photoactive metal chalcogenide compounds consisting of earth-abundant and less toxic elements. A particular interest has been paid to ternary indium-based I–III–VI_2 semiconductors such as copper indium sulfide (CIS) both in the stoichiometric form of $CuInS_2$ and non-stoichiometric Cu–In–S compounds with a varied Cu : In ratio.[5–8]

The chalcopyrite CIS NPs can be prepared with large variations in stoichiometry while preserving the chalcopyrite structure with no additional binary phases.[5–8] Both stoichiometric $CuInS_2$ and non-stoichiometric Cu–In–S NPs reveal broad absorption bands extending to around 800 nm (for bulk $CuInS_2$ the bandgap E_g is 1.5 eV) and quite a high absorption coefficients exceeding 10^5 cm^{-1}.[6,7] At the same time, the CIS NPs are reasonably stable both in the dark and under photoexcitation.[5–7] A combination of these features makes CIS NPs a good candidate as a visible light harvester both for solid-state photovoltaic solar cells and liquid-junction photoelectrochemical solar cells.[5–11] In the latter systems, the CIS NPs act as a spectral sensitizer that absorbs through the entire visible light range

[a]*L. V. Pysarzhevsky Institute of Physical Chemistry, National Academy of Sciences of Ukraine, Laboratory of Organic Photovoltaics and Electrochemistry, 31 Nauky av., Kyiv, 03028, Ukraine. E-mail: alstroyuk@ukr.net; stroyuk@inphyschem-nas.kiev.ua; Fax: +380 44 5250270; Tel: +380 44 5250270*

[b]*V. E. Lashkaryov Institute of Semiconductors Physics, National Academy of Sciences of Ukraine, Kyiv, 03028, Ukraine*

[c]*Semiconductor Physics, Technische Universität Chemnitz, 09107 Chemnitz, Germany*

† Electronic supplementary information (ESI) available: Details of preparation of FTO/TiO_2 films and XPS measurements; absorption and PL spectra of CIS and CIS@ZnS NPs produced at different Zn : Cu ratio and different x_{Cu}, x_{In}, and x_S; *J–V* curves for the FTO/TiO_2/CIS photoanodes produced at different x_{Cu} and x_{In}; survey XPS spectra of CIS NPs and TiO_2/CIS@ZnS heterostructure and high-resolution N1s, In3d, Zn2p, O1s, and C1s XPS spectra of CIS and CIS@ZnS NPs; data on atomic Cu : In fractions in the produced NPs as determined by XPS; SEM images of bare FTO/TiO_2 film as well as FTO/TiO_2/Cu^0 and FTO/TiO_2/Cu_2S heterostructures; distribution of colloidal CIS NPs by the hydrodynamic size and a TEM image of CIS NPs; element maps for FTO/TiO_2/Cu_2S heterostructure determined by EDX. See DOI: 10.1039/c6ra18313a

and injects electrons into a wide-band-gap metal oxide component of the photoanodes.[6,7,9–11] The reported conduction band (CB) edge of CIS NPs is around −0.5 V (*vs.* normal hydrogen electrode (NHE)) for the stoichiometric $CuInS_2$ (ref. 12) and shifts to more negative values for the NPs with a lower molar Cu : In ratio.[12,13] Therefore, the conduction band potential (E_{CB}) of CIS NPs matches almost perfectly the E_{CB} of TiO_2 and ZnO (E_{CB} around −0.5 V *vs.* NHE at pH 7 (ref. 14)), that are typically used in the photoanodes of the liquid-junction solar cells, allowing for efficient photoinduced electron transfer from the CIS NPs to the metal oxide with minimal losses in energy. Alternatively, the CIS NPs can be used as a charge transfer layer in the solid-state solar cells[15] and as a counter-electrode component for the dye-sensitized solar cells[12] as well as photocatalysts of a number of redox processes including dyes degradation[16] and water splitting.[11,17]

As compared to the binary cadmium or lead chalcogenide NPs the range of synthetic strategies applied to produce CIS NPs of a definite size and composition is much narrower. Typically, the Cu–In–S NPs are synthesized by the well-known "hot-injection" method in high-boiling point solvents (such as octadecene or oleylamine) at 200−250 °C in the presence of capping agents with long alkyl chains like dodecanethiol.[5–8,11,18–22] Such NPs reveal a precise control of the size, composition and the thickness of protecting surface shells of ZnS or CdS. However, to be used for the bio-imaging or as the light absorbers the post-synthesis ligand exchange of long-chain stabilizers with smaller molecules is obligatory to make the NPs water-soluble for the bio-diagnostics or to facilitate electron transfer in the solar cells.[6–8,11,18,23,24] In the meantime, the direct and "green" synthesis of CIS NPs with a tailored size and composition in polar solvents, especially in water, remains a challenge.

Similarly to Cd- and Pb-based NPs, the CIS NPS can be stabilized in polar media by small mercapto carboxylic acids.[25–29] For example, water-soluble Cu–In–S NPs covered with a ZnS shell (CIS@ZnS) with a PL quantum yield of up to 40% were produced by the microwave heating using a combination of mercaptoacetic acid (MAA, $HSCH_2COOH$) and sodium citrate as capping agents.[27] A relatively mild synthesis of mercapto acetate-stabilized CIS NPs at 90–120 °C was reported in ref. 28, however, the NPs were produced in the form of a precipitate and cannot, therefore, be deposited directly on the surface of a titania photoanode. The anion of mercaptopropionic acid (MPA, $HSCH_2CH_2COOH$) was also reported to be an efficient stabilizer for CIS NPs both in basic aqueous solutions[25] and in *N*,*N*-dimethylformamide.[26] A synthesis of MPA-capped CIS NPs by decomposition of a single molecular precursor in the N_2 atmosphere and liquid MPA was also reported.[29] It should be noted, that in the solar cells with the TiO_2/CIS photoanodes the presence of an additional $-CH_2^-$ group in the MPA stabilizer molecule as compared with MAA introduces additional distance between the donor (CIS) and acceptor (TiO_2) that may be detrimental to the solar cell performance. Probably, the highest efficiency to date, 7.04%, was reported in ref. 11 for MPA-capped Cu–In–S@ZnS NPs anchored to TiO_2 as photoanode, polysulfide containing aqueous electrolyte and a Cu_2S counter-electrode. However, the production of such photoanodes included elaborate steps of phase transfer and ligand exchange needed to cap the NPs with an MPA layer and anchor them to the hydrophilic titania surface.

In the present work we report on a "green" and one-step synthesis of non-stoichiometric copper indium sulfide and core–shell Cu–In–S@ZnS NPs stabilized by mercapto acetate (MA) anions under the ambient conditions and moderate temperatures not exceeding 100 °C. The CIS NPs were directly loaded onto the nanocrystalline titania and tested as solar cell photoanodes in a system comprising an S^0/S^{2-} redox-shuttle and a Cu_2S-based counter-electrode. We have optimized the composition of Cu–In–S@ZnS NPs to achieve the maximal photocurrent in model three-electrode cells. Then the structure of optimized TiO_2/CIS@ZnS heterostructures was explored by a combination of X-ray photoemission, energy dispersive and Raman spectroscopy and scanning electron microscopy. Finally, we tested the optimized TiO_2/CIS and TiO_2/CIS@ZnS composites as photoanodes of two-electrode solar cells with TiO_2/Cu_2S counter-electrodes and achieved the light-to-current conversion efficiency exceeding 8%.

Material and methods

Indium(III) chloride, copper(II) chloride dihydrate, zinc(II) acetate dihydrate, $Na_2S \times 9H_2O$, concentrated HNO_3, NH_4OH (aqueous 25 wt% solution), MAA, glycerol, ethylcellulose, ethanol (with 6 v% water), *n*-butanol, and glass plates covered with fluorine-doped tin(IV) oxide (FTO) with a specific resistivity of 7 Ohm cm^{-2} were purchased from Sigma-Aldrich and used without further purification. The nanocrystalline TiO_2 P25 was supplied by Evonik Corp.

Preparation of colloidal solutions and electrodes

The colloidal Cu–In–S NPs were synthesized in aqueous solutions and stabilized by MA anions (Scheme 1). In a typical procedure, to 9.5 mL water 0.2 mL aqueous 1.0 M solution of mercaptoacetic acid, 0.1 mL aqueous 0.1 M $CuCl_2$ solution, 0.05 mL aqueous 1.0 M $InCl_3$ solution (containing 0.2 M HNO_3 to avoid hydrolysis) and 0.04 mL aqueous 25 wt% NH_4OH solution were added under intense magnetic reflux. To the produced mixture 0.1 mL aqueous 1.0 M Na_2S solution was added at vigorous stirring and the solution was kept at ~90 °C in a water bath for 20 min. To produce Cu–In–S NPs of a different composition the concentration of copper or indium chloride or sodium sulfide were varied while the concentrations of all other components maintained constant.

The as-prepared CIS colloids were cooled to room temperature divided into two parts. The first part was used without additional modifications for the preparation of photoanodes. The second part of the solutions was treated to modify the surface of CIS NPs with a thin ZnS layer. For this, 0.05 mL 0.1 M zinc(II) acetate solution was added to 5 mL of the colloid (0.001 M Zn^{2+}) and the solution was additionally kept at ~90 °C for 30 min.

To produce the photoanodes 0.15 mL colloidal CIS or CIS@ZnS solution was deposited onto a hot (120 °C) FTO/TiO_2 film (175 mm^2) and the film was dried at this temperature for 5 min (Scheme 1). The procedure was repeated three times (the

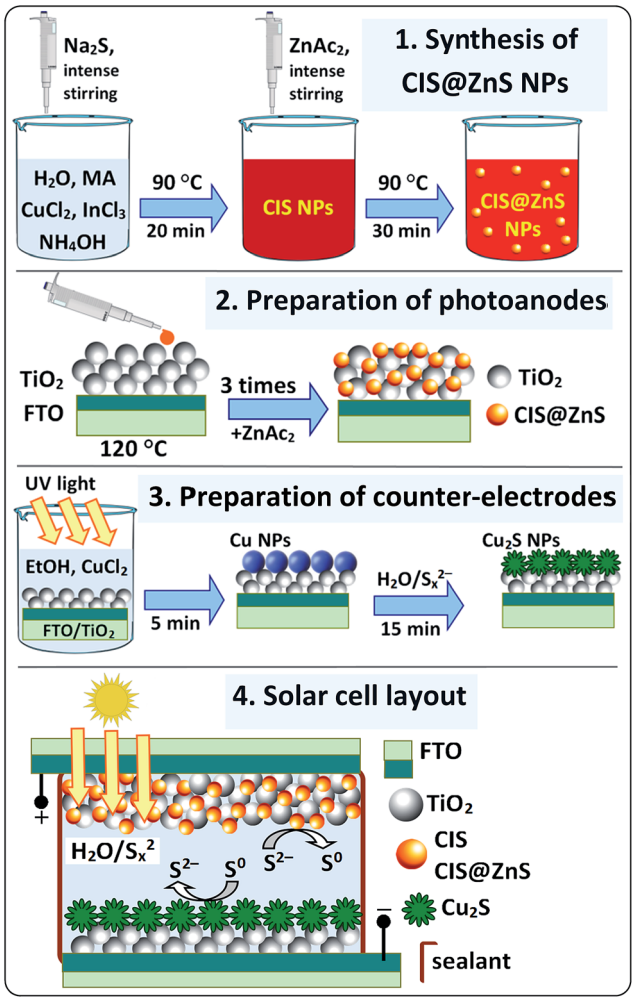

Scheme 1 Schematical description of synthetic procedures and solar cell outline.

repetition number was chosen experimentally to produce the maximal photocurrent density).

The titania films on FTO (FTO/TiO_2) were prepared by the well-known "doctor blade" method and the synthesis details provided in ESI.† The FTO/TiO_2/Cu_xS counter-electrodes were produced by a photoassisted-method similar to that recently introduced by us for ZnO-based cells[30,31] (Scheme 1). In a typical procedure, an FTO/TiO_2 film was immersed into 0.02 M $CuCl_2$ solution in 94 v% ethanol (2 mL) in a quartz 10.0 optical cuvette and illuminated with focused light of a mercury high-pressure lamp in the spectral range of $\lambda > 310$ nm with an intensity of 50 mW cm^{-2} for 5 min from the side of titania and then 5 min from the size of FTO to ensure uniform deposition of the copper NPs. The FTO/TiO_2/Cu_2S films were produced by immersing the as-prepared FTO/TiO_2/Cu^0 samples in aqueous 1.0 M Na_2S_x ($S^0 : S^{2-} = 1 : 1$) solution for 15 min, rinsed with water and dried at ambient conditions.

Instruments

The absorption and photoluminescence (PL) spectra were registered on a Specord 210 spectrophotometer and a Perkin-Elmer LS55 luminescence spectrometer, respectively, in standard 1.0–5.0 mm cuvettes. In order to acquire PL spectra the samples were excited by 450 nm light in standard 10.0 mm quartz cuvettes and the PL was registered at an angle of 90° to the excitation beam.

X-ray photoemission spectroscopy (XPS) investigations were performed with an ESCALAB™ 250Xi X-ray Photoelectron Spectrometer Microprobe (Thermo Scientific). The details of XPS spectra acquisition are provided in ESI.† Raman spectra were excited with the 488 nm line of a solid-state laser (Sapphire, Coherent) or a 325 nm line of He–Cd laser and registered with at a spectral resolution of 2 cm^{-1} using a Lab-Ram HR800 micro-Raman system equipped with the liquid nitrogen cooled CCD detector (Symphony). The incident laser power was kept below 0.02 mW, in order to avoid sample heating under the microscope objective (100× for 488 nm and 40× for 325 nm excitation). For the XPS and Raman measurements, the colloidal NP solutions were drop-casted on a pre-cleaned Si substrate and dried at ambient conditions. The FTO/TiO_2/CIS@ZnS photoanodes were studied after their testing in photoelectrochemical (PEC) systems without additional preparatory procedures.

Scanning electron microscopy (SEM) of the photoanodes was performed using a Tescan Mira 3 LMU microscope with an accelerating voltage of 5–20 kV. Energy-dispersive X-ray (EDX) spectra were taken using a built-in Oxford X-max 80 mm^2 setup.

X-ray diffraction (XRD) patterns of CIS and CIS@ZnS NPs were registered in a range of $2\Theta = 10–100°$ with a step of 0.02° using a Bruker XRD Analyzer D2 Phaser operating with the copper K_α irradiation. To prepare samples for the XRD measurements the original CIS solutions were concentrated by a factor of 10 with a rotary evaporator, the NPs were precipitated by adding 2-propanol, separated by the centrifugation and redispersed in distilled water. The solid samples were then prepared by dropping the concentrated CIS solution onto polished silicon plate and evaporating the water under ambient conditions.

Photoelectrochemical measurements

Photoelectrochemical experiments were carried out in two- or three-electrode configurations. In the three-electrode cells, an FTO/TiO_2/CIS (CIS@ZnS) heterostructure was used as a working photoanode, a Pt wire as a counter electrode and a saturated Ag/AgCl as a reference electrode. An aqueous solution containing 0.1 M Na_2S and 0.1 M Na_2SO_3 was used as an electrolyte. The cells were illuminated from the FTO side of the photoanodes by a metal-halide xenon-filled lamp (OSRAM HMI 200 W/SE) in the range of $\lambda > 320$ nm with the integral light intensity of 30 mW cm^{-2} (measured by a Gentec Solo 2 actinometer). The applied bias was varied from +200 mV to −1200 mV with a rate of −10 mV s^{-1}. The bias application and photocurrent measurements were performed with a Keithley 2400 multimeter. The chronoamperograms were registered at a constant bias (equal to the "dark" immersion potential of the photoanode) and chopped illumination with ~20 s "light-on" and "light-off" periods. All the voltages in the three-electrode scheme are given below relatively to the saturated Ag/AgCl reference electrode.

The two-electrode cells were prepared in the following way (see typical cell layout in Scheme 1). A 1 mm-thick parafilm layer was applied to a hot (120 °C) FTO/TiO_2/CIS (CIS@ZnS) photoanode leaving open a ~0.5 cm^2 window. On top of the parafilm, a hot (120 °C) FTO/TiO_2/Cu_2S counter-electrode was then applied under a mild pressure. After cooling this "sandwich" structure to room temperature two holes were made in the parafilm for electrolyte admission and air release from the cell. The cell was then filled with 1.0 M aqueous Na_2S_x ($S_0 : S^{2-} = 1 : 1$) solution and the cell was sealed with an adhesive commercial sealant. The outer surface of the photoanode was then covered with a black lacquer leaving a window of 0.3 cm^2 for the cell illumination. Such cells demonstrated steady PEC parameters for at least a week without any traces of deterioration. Several identical two-electrode cells were prepared in a similar way and studied in identical conditions to test the reproducibility of the parameters. Illumination of the three- and two-electrode cells was carried out in the same regime. Electrode potentials and photocurrents were measured by a Keithley 2400 multimeter. In the following discussion, we will omit the "FTO/" component to simplify the designation of the heterostructures (*e.g.* TiO_2/CIS instead of FTO/TiO_2/CIS) implying by definition that the FTO is present as a support in all the studied composite electrodes.

Results and discussion

To gain an insight into the effect of the composition of CIS NPs on their photoelectrochemical properties we have studied FTO/TiO_2/CIS heterostructures as photoanodes of model three-electrode solar cells with aqueous Na_2S/Na_2SO_3 electrolyte and a Pt wire as a counter-electrode. The electrolyte was chosen so to avoid the release of S^0 that leads to the Pt poisoning.[9]

Using the photocurrent density as a criterion for optimization of the photoanode composition we varied systematically the content of each constituent of the CIS and CIS@ZnS NPs while maintaining constant contents of other components. The experiments discussed further in details showed that the highest photoelectrochemical activity is observed for the CIS NPs with a molar Cu : In : S ratio of 1 : 5 : 10. This optimal ratio was found by varying the copper content in the "x_{Cu} : 5 : 10" series, the indium content in the "1 : x_{In} : 10" series and the sulfur content in the "1 : 5 : x_S" series, where x_{Cu}, x_{In}, and x_S are molar ratios of the corresponding components. Also, it was found that the "core–shell" Cu–In–S@ZnS NPs produced by the deposition of a thin ZnS shell on the surface of CIS NPs exhibit a much higher activity as a visible-light-sensitive component of the photoanodes as compared to the uncoated NPs and perform in a much more stable and reproducible way than uncovered NPs. The highest activity and stability was observed at a molar Zn : Cu ratio of 1 : 1.

On the second stage of the work, we subjected the optimized CIS and CIS@ZnS NPs and photoanodes produced from such NPs to a detailed study by using X-ray photoemission and Raman spectroscopies as well as SEM and EDX analysis. Finally, the optimized TiO_2/CIS@ZnS heterostructures were tested in the two-electrode solar cells and the basic parameters of the cell performance determined and reported in the present paper.

We found a distinct correspondence between the photoelectrochemical activity of the CIS@ZnS NPs as light harvesters and the luminescent properties of such core/shell NPs. In particular, at a constant Zn : Cu ratio and at a variation of the copper and indium content the PL intensity of core@shell CIS@ZnS NPs in solutions follows the PEC activity of the TiO_2/CIS@ZnS heterostructures produced from such colloids. A detailed account of the luminescent properties of the CIS@ZnS NPs will be a subject of separate contribution and in the present paper we would only stress that the PL properties of CIS@ZnS NPs can be used as an indicator for the design and selection of the absorber NPs to achieve the highest photoelectrochemical activity.

Screening for the optimal composition of CIS@ZnS NPs

Optimal Zn : Cu ratio in the shell. Similarly to the broadly studied cadmium chalcogenide NPs, it was found that the formation of a ZnS shell on the surface of CIS NPs results in drastic enhancement of PL intensity as well as in a considerable growth of the photoelectrochemical activity of NPs coupled to titanium dioxide. In particular, an increase in the molar Zn : Cu ratio from 0 (no zinc) to 20 resulted in a more than 30-fold increment of the PL efficiency (Fig. 1a, curve 1). The photocurrent measured for the TiO_2/CIS@ZnS photoanodes based on such NPs in the three-electrode cells was found to increase from around 2.0 mA cm^{-2} for uncovered Cu–In–S NPs to 2.5 mA cm^{-2} for the core/shell NPs with a Zn : Cu ratio of 1 : 1 (Fig. 1a, curve 2). As opposite to the PL properties, further increase of the Zn content results in deterioration of the PEC activity of CIS@ZnS NPs and for the thickest ZnS shell and the highest PL efficiency, at Zn : Cu = 20 : 1, the photocurrent density is three times lower than for the original uncovered CIS NPs. The deterioration effect on PEC activity seems to be general for CIS NPs covered with a different metal-sulfide shell. For example, a lowering of the PEC activity with increasing shell thickness was reported for CIS@ZnS and CIS@CdS NPs.[22] Between those two shells, an increase in zinc sulfide shell thickness had a much stronger effect because of a much higher barrier between the E_{CB} levels of CIS and ZnS reaching ~1 eV.[22]

Apart from the PL enhancement, the doping of Cu–In–S NPs with zinc(II) occurs resulting in a blue shift of the absorption band edge (ESI, Fig. S1a†) and a concomitant shift of the PL band maximum (Fig. S1b†). Also, a spectral shoulder at 440–450 nm characteristic for mixed-phase non-stoichiometric Cu–In–S NPs (see discussion below) also disappears indicating considerable changes in the composition and electronic properties of such Cu–In–S@ZnS NPs. These phenomena are well reported and caused by penetration of Zn^{2+} ions into the Cu–In–S core resulting in the lattice reconstruction and a bandgap widening.[7,11,25]

The dependencies given in Fig. 1a can be understood by assuming that the deposition of a ZnS shell results in the elimination of structural defects acting as surface sites of radiationless recombination. At that, the competing processes

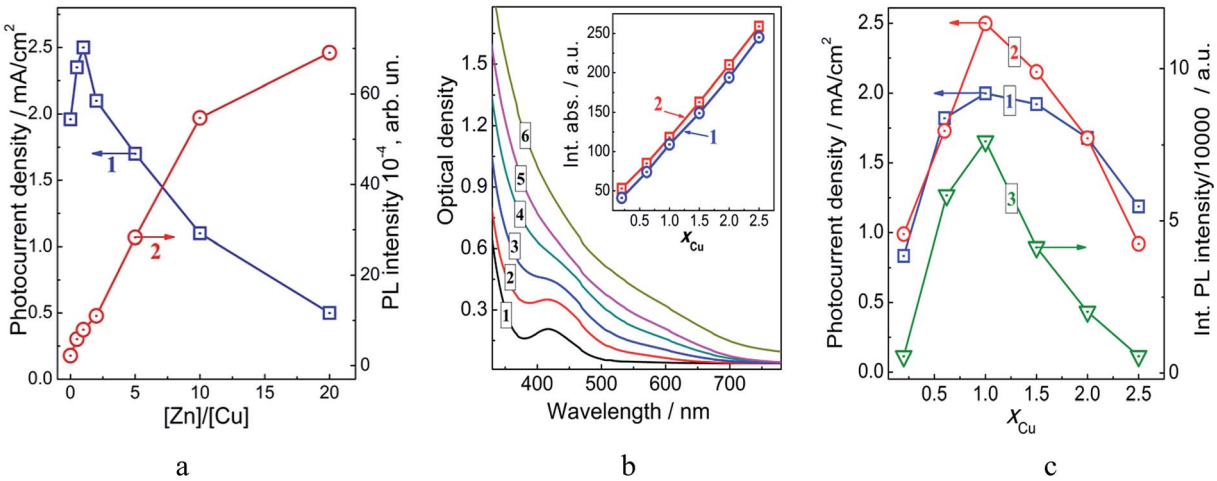

Fig. 1 (a) Photocurrent density J (curve 1) obtained for TiO_2/CIS@ZnS photoanodes and PL intensity of CIS@ZnS NPs (curve 2) as a function of molar Zn : Cu ratio during the ZnS shell deposition. (b) Absorption spectra of CIS@ZnS NPs produced at fixed In and S contents and a varied molar ratio Cu : In : S = x_{Cu} : 5 : 10 with x_{Cu} = 0.2 (curve 1), 0.6 (2), 1.0 (3), 1.5 (4), 2.0 (5), and 2.5 (6). Inset in (a): integral absorbance of CIS NPs (curve 1) and CIS@ZnS NPs (2) as a function of x_{Cu}. (c) Photocurrent density J (curves 1 and 2) obtained for TiO_2/CIS (1) and TiO_2/CIS@ZnS (2) photoanodes and PL intensity of CIS@ZnS NPs (curve 3) as a function of x_{Cu}.

of the radiative electron–hole recombination in CIS@ZnS NPs and the interfacial electron transfer in the TiO_2/CIS@ZnS heterostructures become much more efficient resulting in the PL enhancement and the photocurrent increase. However, as the ZnS shell becomes thicker it impedes the interfacial electron transfer and promotes at the same time the electron–hole recombination in the CIS core. Therefore, at a higher ZnS content, we observe a sharp decrease of the PEC activity of the TiO_2/CIS@ZnS heterostructures with a steady growth of the PL intensity of core/shell CIS@ZnS NPs used for the preparation of the photoanodes. As can be seen from Fig. 1a, the PEC measurements showed that the peak photocurrent density is achieved at a comparatively low Zn(II) content, that is, for a relatively thin ZnS shell on the surface of CIS NPs. At a Zn : Cu ratio of 1 : 1 (optimal for the PEC performance) the absorption spectra of uncovered and core/shell NPs are essentially identical (compare spectra in Fig. 1a, curves 1 and 2 and Fig. S2a, ESI†) indicating that the Zn(II) doping effect is small to negligible and can be ignored in such conditions. In view of these observations, all the following studies on dependencies between the composition of CIS@ZnS NPs and their photoactivity were performed with the molar ratio of Zn : Cu = 1 : 1.

Optimal x_{Cu} in the core Cu–In–S NPs. It was found that an increase of copper content in the CIS NPs results in a gradual transformation of the structure of the fundamental absorption band of colloidal NPs and a general growth of the absorbance in UV and visible spectral range (Fig. 1b). Similar spectral changes have recently been observed by P. V. Kamat *et al.*[32,33] for 2.5 nm CIS NPs with a varied copper content. In particular, they reported that a decrease in Cu content is accompanied by the gradual extinction of the band edge absorption around 680 nm and formation of a distinct new band peaked at around 500 nm. Basing on the stationary and time-resolved spectral observations they assigned the latter band to a size-quantized interband transition, while the longer wavelength absorption was associated with intragap transitions with the participation of Cu^{2+}/Cu^{+} centers.

The spectral changes observed in the present work agree well with the results reported in ref. 32. As the x_{Cu} increases the contribution of Cu-center-associated absorption increases as well and the tendency is reflected in the formation of a longer-wavelength tail at λ > 500 nm and masking of the interband absorption band at λ < 500 nm. For each given x_{Cu} the absorption spectra of uncovered and core/shell NPs were almost identical varying slightly in intensity (compare Fig. 1b and S2a, ESI†). The integral absorbance of the colloidal solutions was found to increase in a linear manner with an increase of copper content and the corresponding dependencies were found to be quite close both for the uncovered and core/shell NPs (Fig. 1b, inset).

The intragap Cu-related centers can participate in the radiative electron–hole recombination[7,20,32,33] observed as the PL emitted in a broad band with a maximum shifting to longer wavelengths as the x_{Cu} increases (ESI, Fig. S2b†).

Both types of NPs reveal also similar dependences of the photoelectrochemical activity on the composition (Fig. 1c). The photocurrent density generated by the TiO_2/CIS@ZnS photoanodes increases as the x_{Cu} grows from 0.2 to 1.0, then it peaks at a NP composition corresponding to Cu : In : S = 1 : 5 : 10 and decreases at x_{Cu} = 2.5 almost to the same value as for the NPs with the minimal copper content (original J–V characteristics of the copper-varied photoanodes are provided in ESI, Fig. S3†). No positive PEC response was obtained from FTO/TiO_2/In_2S_3 heterostructures produced in a similar way but without the addition of copper ions. The indium sulfide NPs exerted only a light screening effect diminishing the PEC response of the FTO/TiO_2 film.

For the most active absorber NPs with $x_{Cu} = 1.0$ the increment of PEC activity introduced by the ZnS shell deposition reaches around 25% (compare curves 1 and 2 in Fig. 1c). It should be noted that the dependence of the integral PL intensity of Cu–In–S@ZnS NPs on the x_{Cu} follows closely the relationship between the PEC activity and copper content and reaches the maximal value at $x_{Cu} = 1.0$ as well, dropping quite considerably at a higher copper content (Fig. 1c, curve 3). The PL intensity is therefore in this case a good indicator allowing to anticipate the PEC activity of colloidal CIS NPs basing on the spectral data.

Optimal x_{In} in the core Cu–In–S NPs. The value of x_{In} was varied at $x_{Cu} = 1.0$ and $x_S = 10$ in the range of 1–6 (Fig. 2a). At a lower x_{In}, the copper sulfide NPs can readily form, while an increase of indium(III) content higher than $x_{In} = 6$ has a little effect on the PEC activity and optical properties of CIS and CIS@ZnS NPs. The absorption and PL spectra of CIS@ZnS NPs produced within this series are presented in ESI in Fig. S4.† At a low In content, copper-rich phases form that exhibit no characteristic shoulder at 440–450 nm (Fig. S4a†). Corresponding PL bands are situated in a longer wavelength range with the maxima at 700–750 nm as typical for the Cu-rich NPs (compare with Fig. S2b†). With increasing x_{In} the absorption spectrum acquires gradually the characteristic shape with a shoulder feature at around 440 nm while the PL band shifts to the shorter wavelength. The maximal PL efficiency is observed for the NPs with Cu : In : S = 1 : 5 : 10 while at a higher x_{In} it drops to some extent.

We can expect therefore that the maximal PEC activity would be shown by the TiO_2/CIS@ZnS NPs produced at $x_{In} = 5.0$ and the NPs poorer and richer for indium would be less active. Fig. 2a shows these expectations to be quite correct. The dependences of PEC activity for both CIS and CIS@ZnS based photoanodes show an increasing trend with increasing x_{In}, reach the maxima at $x_{In} = 5.0$ and then come to some drop similarly to the corresponding dependence of PL intensity (original J–V characteristics of the indium-varied photoanodes are provided in ESI, Fig. S5†).

Optimal x_S in the core CIS NPs. The optimal x_S was searched in the range of 7–15 (Fig. 2b) with x_{Cu} and x_{In} fixed at 1.0 and 5.0, respectively. At a lower sulfide content, the colloidal solutions appear unstable toward coagulation. The absorption spectra of original CIS@ZnS colloids in this series (ESI, Fig. S6a†) show the structure typical for mixed-phase non-stoichiometric copper indium sulfide with a shoulder at 440–450 nm and a non-distinct edge at 650–700 nm indicative of intra bandgap electron transitions.

The PL band maximum reveals a blue shift with increasing x_S indicating the formation of Cu-poorer phases while the PL intensity decreases steadily with an increase in the sulfide content (ESI, Fig. S6b†). The absorption spectra of CIS@ZnS NPs (ESI, Fig. S6a†) are more or less the same in the range of $x_S = 7$–15 indicating that the formation of core CIS NPs is almost complete already at $x_S = 7$ and at a higher x_S an excess of free sulfide ions is present in the colloidal solution. In view of this fact the decrease of PL intensity of CIS@ZnS NPs at an increasing Na_2S content (Fig. 2b, curve 3) can be associated with the homogeneous nucleation of ZnS NPs in a reaction between Zn^{2+} and S^{2-} in solution rather than the deposition of a ZnS shell on the surface of CIS NPs. The probability of such homogeneous nucleation increases with an increase of x_S prohibiting the "healing" of the surface sites of radiationless recombination by the ZnS shell and thus decreasing the probability of PL emission.

The photocurrent density produced by the TiO_2/CIS and TiO_2/CIS@ZnS photoanodes (Fig. 2b, curves 1 and 2, respectively) increases till $x_S = 10$ and then lowers slightly in the range of $x_S = 10$–15. The maximal PEC activity was observed for $x_S = 10$ both for CIS and CIS@ZnS light absorbers.

Summarizing this section, we found that the maximal PEC activity among the studied samples is observed for the TiO_2/CIS@ZnS heterostructure with the composition of absorber NPs corresponding to Cu : In : S = 1 : 5 : 10 and the shell composition corresponding to a Zn : Cu ratio of 1 : 1. Maintaining these proportions the concentration of the colloidal CIS solutions can be varied in a reasonably broad range producing the NPs with identical optical and PEC properties irrespectively of the concentration of original colloid. In the following section, we present the results of a detailed characterization of such CIS (CIS@ZnS) NPs and the TiO_2/CIS@ZnS photoanodes.

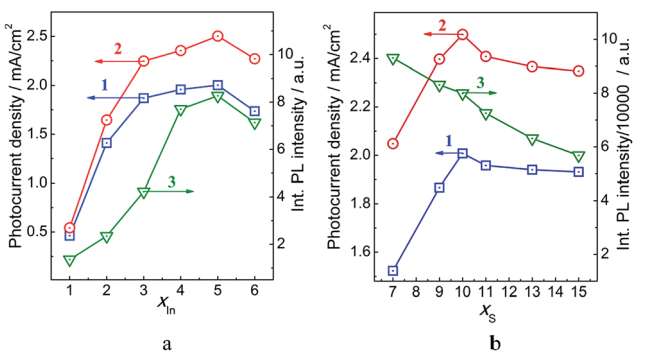

Fig. 2 Photocurrent density J (curves 1 and 2) obtained for TiO_2/CIS (1) and TiO_2/CIS@ZnS (2) photoanodes and PL intensity of CIS@ZnS NPs (curve 3) as a function of x_{In} (a) and x_S (b).

Characterization of optimized "core" CIS, "core/shell" CIS@ZnS NPs and corresponding FTO/TiO_2/CIS@ZnS heterostructures

XPS and XRD characterization. A survey XPS spectrum of the CIS NPs synthesized at a Cu : In : S ratio of 1 : 5 : 10 (ESI, Fig.-S7a,† curve 1) exhibits signals from Cu, In, S, O, N, and C from the constituents of the colloidal particles, that is from the Cu–In–S core surrounded by a shell of adsorbed mercapto acetate stabilizer. The N1s XPS signal of CIS NPs (ESI, Fig. S7b†) can be deconvoluted into three components peaked at 399.9 eV, 401.1 eV, and 407.0 eV. The peaks were assigned to the adsorbed NH_3, NH_4^+ cation and NO_3^- anion, respectively,[34,35] all the three species residual from the NP synthesis. Additionally, a NaCl admixture can be found originating from salt residuals. In the XPS survey spectrum of CIS@ZnS NPs loaded on the titania film additional signals from Zn and Ti can be detected (ESI, Fig. S7a,† curve 2).

The measurements of Cu and In content in the CIS and CIS@ZnS NPs, as well as TiO_2/CIS and TiO_2/CIS@ZnS heterostructures showed that the Cu : In ratio is close to 1 : 5 in all three samples and corresponds to the Cu : In : S ratio set by the starting reagent concentrations (ESI, Table S1†).

A high-resolution section of the XPS spectrum of Cu–In–S NPs corresponding to the In3d is given in ESI (Fig. S8†). The In3d section exhibits a doublet at 444.1/451.7 eV with a splitting of 7.6 eV characteristic for In(III).[12,28,36,37] The peak positions are typical for trivalent indium in ternary copper–indium chalcogenides.[33,34] The Cu2p section of the XPS spectrum reveals a doublet at 931.4/951.3 eV (Fig. 3a) with a splitting of 19.9 eV typical for copper(I)[12,28,37] attesting to the fact that original Cu^{2+} is reduced (either by mercaptoacetic acid or by sulfide ions) and introduced as Cu^{+} into the Cu–In–S NPs. The In3d and Cu2p spectra of CIS, CIS@ZnS, and TiO_2/CIS@ZnS samples are identical indicating unaltered In(III) and Cu(I) states after the deposition of a ZnS shell and anchoring of the CIS@ZnS NPs to the surface of titania films. After the ZnS shell deposition, a Zn-related doublet at 1021.2/1044.2 eV appears (ESI, Fig. S9†) with a splitting of 23 eV characteristic to Zn(II).[34–36]

The O1s band in the XPS spectrum of Cu–In–S NPs (ESI, Fig. S10,† curve 1) can be deconvoluted into three components peaked at 530.7 eV, 531.9 eV, and 534.9 eV, that were assigned to oxygen in C–OH and C=O groups in the carboxylate group of MA anions and to the adsorbed water, respectively.[34,35] In the O1s range of the Cu–In–S@ZnS NPs anchored to the titania surface (Fig. S10,† curve 2) an additional peak at 529.3 eV can be resolved corresponding to the lattice oxygen in TiO_2. The positions of C–OH/C=O related peaks are shifted to 531.0 and 533.1 eV, respectively, most probably, reflecting the formation of hydrogen bonds between the carboxylate group of MA stabilizer of CIS@ZnS NPs and the TiO_2 surface. Additionally, the intensity ratio of these peaks is increased considerably reflecting most probably a contribution of Ti-OH groups on the surface of titania film left free from the adsorbed NPs.

The C1s band of CIS NPs can be deconvoluted into three components with maxima at 284.5 eV, 285.6 eV, and 288.3 eV (ESI, Fig. S11,† curve 1) that can be assigned to single bonded C–C carbon in MA ions and/or adventitious carbon, C bonded to SH and OH groups, and C in carboxylate groups, respectively.[34,35,37] After deposition on the TiO_2 surface, the latter signal splits into two peaks at 287.8 eV and 288.9 eV (Fig. S11,† curve 2) that can be ascribed to the partial binding of the carboxylate group of MA to the titania surface *via* hydrogen bonds.

The S2p band of CIS NPs is a combination of two doublets (Fig. 3b, curve 1) at 161.4/162.6 eV and 163.1/164.3 eV with a characteristic spin–orbit splitting of 1.2 eV.[34,35] The first component can be assigned to sulfur in the lattice of Cu–In–S NPs.[28] Similar signals were observed for the lattice anions of $CuFeS_2$ chalcopyrite.[35] The doublet at 163.1/164.3 eV can be assigned to thiol sulfur, that is the C–SH group of mercapto acetate stabilizer adsorbed on the NP surface.[34,35]

The S2p spectrum of TiO_2/CIS@ZnS heterostructure is quite different. In this case, three doublets can be deconvoluted – at 160.8/162.0 eV, 161.4/162.6 eV, and 167.5/168.7 eV (Fig. 3b, curve 2). The first doublet is located in the area typical for simple metal sulfides like ZnS, CdS, and PbS[34,35] and can, therefore, be assigned to the sulfur atoms in the ZnS shell. The second doublet, similarly to the original CIS NPs, can be ascribed to the lattice sulfur of copper indium sulfide. No thiol sulfur can be observed in this case indicating that the adsorbed MA was mostly substituted in the process of the ZnS shell formation. The doublet at 167.5/168.7 eV can be assigned to SO_x species, that is, to the products of sulfide oxidation.[28] The same signal appears in the S2p XPS spectrum of colloidal CIS NPs subjected to prolonged thermal treatment on air (not shown).

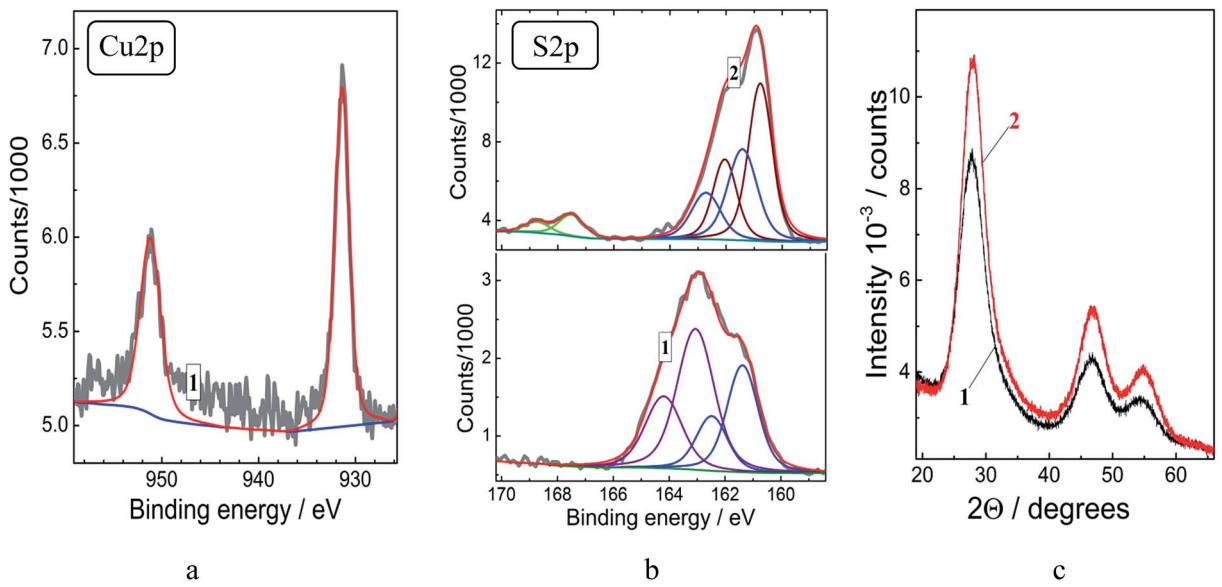

Fig. 3 (a and b) High resolution X-ray photoelectron spectra of CIS NPs (curves 1) and CIS@ZnS NPs in the TiO_2/CIS@ZnS photoanode (curve 2) in the range of Cu2p (a) and S2p signals (b). (c) X-ray diffraction patterns of CIS NPs (curve 1) and CIS@ZnS NPs (curve 2).

The presence of this signal for the TiO_2/Cu–In–S@ZnS heterostructure can be accounted for by partial photocorrosion of the CIS NPs exposed to weak ambient light prior to the XPS measurements.

The XRD pattern of CIS NPs revealed broadened reflections peaked at $2\Theta = 27.7°$, 31.5°,46.7° and 54.4° (Fig. 3c, curve 1) that can be indexed as (112), (200), (204/220), and (312) planes of the tetragonal chalcopyrite CIS (JCPDS #65-2732, 27-0159), respectively. The close position of the XRD reflections of the Cu-poor NPs studied here to the stoichiometric CIS NPs is a typical phenomenon observed for a broad range of the Cu–In–S NP compositions.[25,23,33] The deposition of a thin ZnS shell does not alter the general structure of the CIS NPs (Fig. 3c, curve 2) resulting only in a slight shift of the reflections to 27.9°, 31.8°, 46.9°, and 54.7°. The shift is an indication of some doping of the CIS NP core with Zn^{2+} ions thus confirming the formation of a ZnS shell on the surface of CIS core NPs.[25,27] A more detailed assignment of the XRD reflections to specified CIS phases, such as, for example, $CuIn_5S_8$, is impossible due to a large width of the reflections indicating a small size of the CIS crystallites. Estimations made using the Scherrer equation showed that the coherent X-ray scattering domain (the CIS crystallite size) is 3–4 nm for both CIS and CIS@ZnS NPs, in accordance with the TEM results discussed below.

Characterization by Raman spectroscopy. We performed Raman study on the drop-casted film samples and powders of initial bare CIS NPs, CIS@ZnS NPs, and TiO_2/CIS@ZnS heterostructure used as a solar cell photoanode. The Raman spectra were measured at two excitation wavelengths: $\lambda_{exc} = 488$ nm (2.5 eV) that is resonant for CIS and $\lambda_{exc} = 325$ nm (3.8 eV) that is resonant for ZnS. The reason for using the latter λ_{exc} was to distinguish the ZnS shell formation from alloying Zn into the CIS lattice. This is intrinsically a tricky task, but the recent results showed that the Raman spectroscopy is a promising method for such speciation. For example, this approach was successfully employed for identification of ZnS as a secondary phase in Cu_2ZnSnS_4 (ref. 38 and 39) and distinguishing the ZnS shell formation from Zn alloying into CIS[40] or In_xS NPs.[41]

The spectrum of pristine CIS NPs at $\lambda_{exc} = 488$ nm is dominated by a broad complex feature at 240–400 cm^{-1} (Fig. 4a, curve 1). This is the range of previously reported Raman modes of stoichiometric chalcopyrite and wurtzite $CuInS_2$ NPs (260 cm^{-1}, 290 cm^{-1}, 300 cm^{-1}, 320 cm^{-1}, and 350 cm^{-1}),[42,43] stoichiometric $CuIn_5S_8$ (270 cm^{-1}, 325 cm^{-1}, 340 cm^{-1}, and 360 cm^{-1}),[44] as well as non-stoichiometric Cu–In–S NPs of a varied composition.[45]

The weaker and even broader scattering band between 500 and 750 cm^{-1} (Fig. 4a, curve 1) can be related to second-order scattering processes. The CIS NP spectrum recorded at $\lambda_{exc} = 325$ nm has a similarly broad band in the range of 240–400 cm^{-1} (Fig. 4b, curve 1). Some additional scattering feature seen between 400 and 500 cm^{-1} in both CIS and CIS@ZnS samples at UV excitation cannot be assigned at the moment. The Raman spectrum of TiO_2/CIS@ZnS heterostructure at $\lambda_{exc} = 488$ nm (Fig. 4a, curve 2) is a combination of a broad CIS-related band of CIS@ZnS NPs at 240–400 cm^{-1} and three sharper peaks of anatase TiO_2 (marked by the asterisks). This measurement

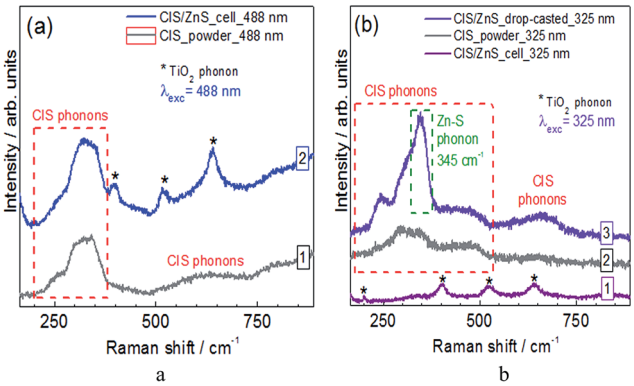

Fig. 4 (a) Raman spectra of CIS NPs (curve 1) and TiO_2/CIS@ZnS heterostructure (2) excited with "CIS-resonant" $\lambda_{exc} = 488$ nm. (b) Raman spectra of TiO_2/CIS@ZnS (curve 1), CIS NPs (2) and CIS@ZnS NPs (3) registered with "ZnS-resonant" $\lambda_{exc} = 325$ nm.

confirms that the CIS@ZnS NPs generally preserve their internal structure upon being built into the heterostructures. Due to a small film thickness of the CIS@ZnS NPs in the TiO_2/CIS@ZnS heterostructure, the corresponding Raman spectrum excited with $\lambda_{exc} = 325$ nm is dominated by the TiO_2-related peaks (Fig. 4b, curve 1). Nevertheless, the Raman spectrum taken with $\lambda_{exc} = 325$ nm (resonant for ZnS) on a drop-casted CIS@ZnS NP film (Fig. 4b, curve 3) shows a distinct peak at 345 cm^{-1} which is a characteristic frequency of ZnS.[38,40] Importantly, observing this phonon peak enhanced at a λ_{exc} resonant with ZnS allows us to distinguish formation of the ZnS shell on the CIS NPs from Zn alloying into the CIS lattice.

SEM characterization of the FTO/TiO_2/Cu–In–S@ZnS heterostructures. To gain insight into the morphology and composition of the photoanodes based on CIS NPs the heterostructures were studied by a combination of SEM and EDX spectroscopy. Fig. 5 (upper part) shows a set of SEM images of the TiO_2/CIS@ZnS photoanode prepared at an optimum Cu : In : S and Zn : Cu ratios of 1 : 5 : 10 and 1 : 1. Prior to the SEM/EDX measurements, the film was tested as a photoanode in a 120 min continuous illumination trial (see Fig. 7a, curve 1). The frontal and cross-sectional SEM images and the film composition as revealed by the EDX analysis were found to be the same for as-prepared and used CIS-based photoanodes. Similarly, the Cu_xS-based counter-electrodes preserved their morphology and composition unchanged after testing in the solar cells.

The film is macroscopically dense without cracks and visible gradients of mass. The higher-magnification images show that the film is porous with both macropores and mesopores, the latter produced by the loose aggregation of the separate titania nanocrystallites. The size of TiO_2 particles estimated using the right side SEM image is around 20–30 nm matching well the reported grain size of the original Evonik P25 TiO_2 used for the film preparation.

The SEM images of bare FTO/TiO_2 film used for the preparation of the photoanodes are provided in Fig. S12 in ESI.† A comparison of Fig. 5 and S12 (ESI†) shows that the deposition of CIS@ZnS NPs does not change appreciably the morphology of the photoanodes. No separate CIS@ZnS NPs can be

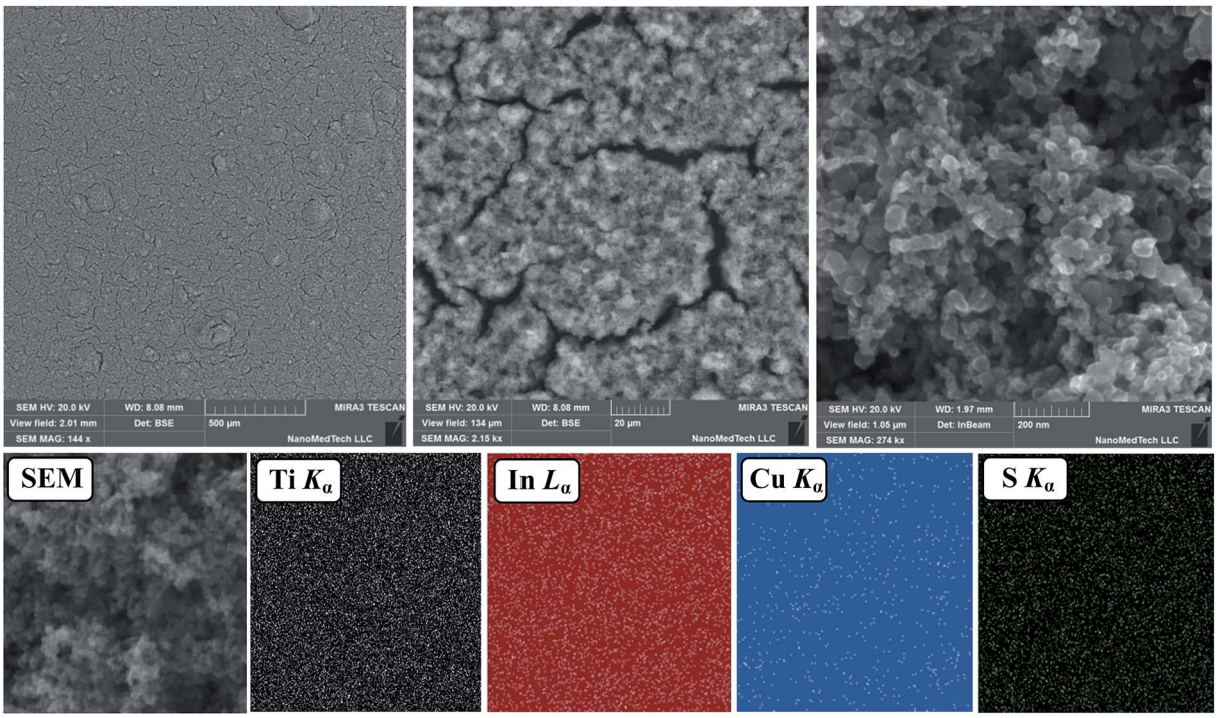

Fig. 5 Frontal SEM images of TiO_2/CIS@ZnS heterostructure registered at a different magnification (upper part) and titanium, indium, copper and sulfur element distribution maps (lower part) for a lower-left side SEM image produced by EDX analysis.

distinguished on the surface of nanocrystalline titania indicating that the size of CIS NPs is much smaller than the grain size in the nanocrystalline P25 TiO_2.

As suggested by the results of dynamic light scattering spectroscopy, the average hydrodynamic size of CIS@ZnS NPs of the optimized composition in original colloidal solutions is around 7–8 nm (ESI, Fig. S13a†) and therefore the real NP size can be evaluated as being 4–5 nm. An examination of the CIS colloid by the transmission electron microscopy revealed strongly agglomerated NP assemblies where separate 3–5 nm particles can be discerned (ESI, Fig. S13b†), in accordance with DLS and XRD results presented above.

The EDX analysis of the TiO_2/CIS@ZnS film surface revealed the presence of Ti, O, Cu, In, S, and Zn with the copper-to-indium ratio being very close to 1 : 5 as set during the synthesis of starting CIS NPs. As the element distribution maps show (Fig. 5, lower part) the Cu, In and S atoms are distributed evenly on the surface of the TiO_2 host matrix mimicking closely a contrast variation of the corresponding SEM image.

A cross-sectional SEM image of the TiO_2/CIS@ZnS (Cu : In : S = 1 : 5 : 10) heterostructure (Fig. 6a) allows to clearly distinguish a 13–14 μm porous layer of the photoactive phase residing on a contrast and dense ~0.5 μm FTO layer. The EDX mapping of copper, indium, and sulfur, along with titanium as a reference (Fig. 6b) shows a uniform distribution of the CIS@ZnS NPs through the bulk of the films from the FTO layer up to the film surface. The fact attests to a homogeneous distribution of the sensitizer NPs in the titania film volume indicating even penetration of the NPs into the film bulk through the pores.

The EDX analysis of the TiO_2/CIS@ZnS film made in five arbitrary points with a different distance from the FTO layer to the film surface (marked as yellow circles in Fig. 6c) showed that the Cu : In ratio is close to 1 : 5 in all the studied points (Table 1). The fact indicates that the sensitizer NPs anchored to the photoanode retain the stoichiometry set by the concentration ratio at the synthesis of original Cu–In–S NPs and their covering with a ZnS shell which is in accordance with the above-discussed XPS results.

Photoelectrochemical properties of the optimized solar cell

The photoelectrochemical properties of TiO_2/CIS@ZnS heterostructures with the optimized composition, that is at the molar Cu : In : S and Zn : Cu ratios of 1 : 5 : 10 and 1 : 1 were studied in two-electrode cells with the copper indium sulfide-based composites as photoanodes and TiO_2/Cu_2S heterostructures produced by the photoassisted approach similar to ref. 30 and 31 as counter-electrodes. The copper sulfide-based counter-electrodes were widely recognized as superior for aqueous polysulfide electrolytes as compared to conventional Pt,[4,14] including the solar cells based on CIS NPs.[7,11]

Earlier we have shown that the ZnO/Cu_xS heterostructures can be used as efficient counter-electrodes with ZnO/CdS photoanodes in polysulfide-based liquid-junction solar cells.[30,31] At that, the ZnO/Cu_xS heterostructure produced by consecutive photocatalytic deposition of copper NPs onto the surface of zinc oxide and sulfurization of ZnO/Cu^0 composite *in situ* in the polysulfide electrolyte appeared to be a much more efficient counter-electrode as compared with similar

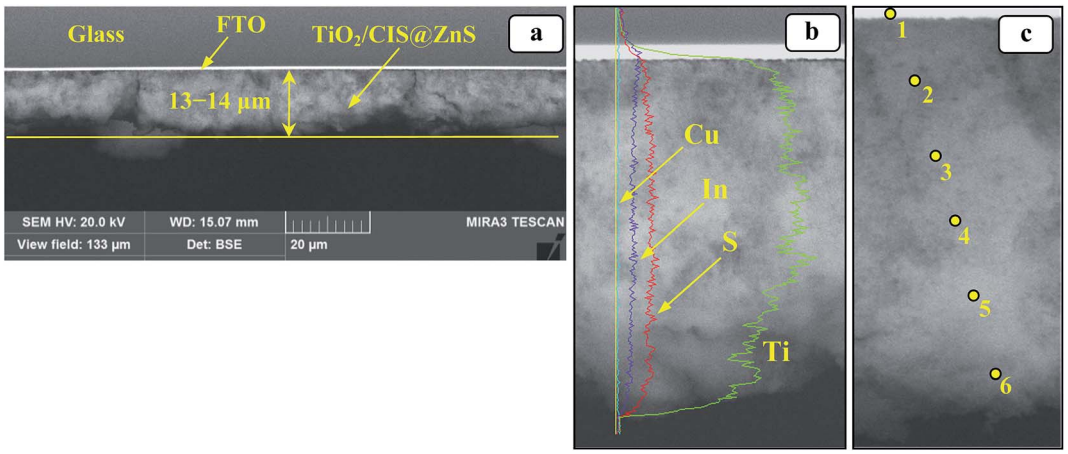

Fig. 6 Cross-sectional SEM images of TiO_2/CIS@ZnS film with EDX signal intensities for different elements (b) and spots chosen for EDX analysis along the film thickness (c). The spot numbers in (c) correspond to the column numbers in Table 1.

Table 1 Copper and indium content in several selected spots of the FTO/TiO2/CIS@ZnS film depicted in Fig. 6

N	1	2	3	4	5	6
Cu, at%	0	0.2	0.2	0.2	0.3	0.2
In, at%	0	1.0	1.1	1.0	1.4	1.1
Cu : In	—	1 : 5.0	1 : 5.5	1 : 5.0	1 : 4.7	1 : 5.5

ZnO/Cu_xS heterostructure produced by conventional two-step ion exchange procedure. Here we extend this approach to the titania-based cells and propose utilization of TiO_2/Cu_2S heterostructures as efficient counter-electrodes for TiO_2/CIS@ZnS-based solar cells. Such titania–copper sulfide heterostructures can also be easily prepared by the two-step method including photocatalytic deposition of Cu NPs onto the titania surface followed by sulfurization of copper NPs in a polysulfide solution (Scheme 1). Within this approach, we can use two identical TiO_2 films for the production of both a photoanode and a counter-electrode.

As shown in ESI (Fig. S14†) the photocatalytic reduction of copper(II) with ethanol on the surface of TiO_2 under illumination with UV light results in the deposition of Cu NPs with a size of around 50 nm and higher that can be easily distinguished on the background of less contrast and smaller titania nanocrystallites (compare Fig. S12 and S14, ESI†). Sulfurization of such films results in the formation of larger, around 100–300 nm, aggregates of separate copper sulfide platelets (ESI, Fig. S15†) with a platelet size of around 50–100 nm and a thickness of less than 20 nm. The integral EDX analysis from the film surface (ESI, Fig. S16†) showed that the atomic Cu : S ratio in the sulfidized film is 2 : 1. The atomic distribution maps of Cu and S mimic closely the distribution maps of Ti and O as well as the morphology of the film indicating a uniform distribution of copper sulfide over the titania surface.

The two-electrode cells based on the TiO_2/CIS@ZnS photoanodes and TiO_2/Cu_2S counter-electrodes were illuminated through the FTO-side of photoanodes with the unfiltered light ($\lambda > 320$ nm after passing through the glass layer of FTO) with an intensity of 30 mW cm^{-2} as described in Materials and Methods. Illumination of the cell results in a shift of the immersion potential of the photoanode by around 0.6 V to more negative values and generation of the photocurrent with the density of around 9–10 mA cm^{-2} (Fig. 7, Table 2).

Under illumination with the chopped light, the photocurrent generation follows closely the light on/off cycles (Fig. 7a, curve 1) clearly indicating that the current originates from the photoexcitation of the cell and the background "dark" current is negligible. Testing of the cell for a considerably prolonged time lapse, around 130 min with the stationary illumination (Fig. 7a, curve 2) showed that in the first minutes of performance the representative cell produced a higher photocurrent of 11.0–11.5 mA cm^{-2} which then drops in ~10 min to ~9 mA cm^{-2} and such value remains more or less steady for at least two hours of illumination. These observations indicate that the cell under investigation is quite robust and chemically stable in the

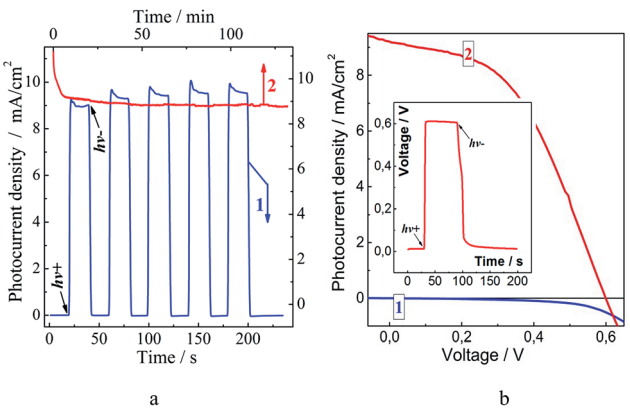

Fig. 7 (a) "Photocurrent–time" dependencies registered at chopped (curve 1) and continuous (2) illumination of the optimized solar cell within different time lapses. (b) "Photocurrent–voltage" and "photopotential–time" (inset) dependencies for the optimized solar cell. Curve 1 is registered in dark, curve 2 – under illumination. "$h\nu$+" and "$h\nu$–" correspond to illumination on and off moments.

Table 2 The photoelectrochemical parameters of the cells based on TiO_2/CIS@ZnS photoanodes with the optimized composition (Av. stands for "average")

	N	J_{sc}, mA cm^{-2}	V_{oc}, V	FF	η, %
Cu–In–S	1	6.6	0.608	0.41	5.76
	2	6.6	0.584	0.46	5.81
	3	6.4	0.595	0.45	5.60
	Av.	6.5	0.596	0.44	5.72
Cu–In–S@ZnS	3	9.2	0.600	0.44	8.10
	4	10.4	0.595	0.39	8.04
	5	10.1	0.612	0.40	8.22
	6	9.2	0.608	0.44	8.20
	7	9.4	0.586	0.42	8.19
	8	9.5	0.595	0.43	8.15
	Av.	**9.6**	**0.600**	**0.42**	**8.15**

studied photoexcitation conditions. It should be noted, however, that the cells were tested under light flux of 30 mW cm^{-2}, which is lower than typically used irradiation of a standard solar simulator (100 mW cm^{-2}) and the values of total light conversion efficiency η reported further in the paper can be regarded as estimations at the present time. Further work is in progress in our group to study the TiO_2/Cu–In–S@ZnS/S_x^{2-}/TiO_2/Cu_2S cells in the standard AM1.5 illumination conditions and obtain the certified efficiency values.

Typical "applied voltage/photocurrent density" curves for the cell in the dark and under the illumination are presented in Fig. 7b. Analysis of such curves allowed to extract basic PEC parameters of the studied cells, that is the short-circuit photocurrent J_{sc} (measured at the zero voltage), the open-circuit photovoltage V_{oc} (measured at the zero photocurrent density), the fill factor FF, and the total light-to-current conversion efficiency η using the well-known equations.[4,14] The results are presented in Table 2 for three identical solar cells produced from uncovered CIS NPs (num. 1–3) and for six identical cells with CIS@ZnS NPs as a light absorber (num. 3–8). It should be also noted that for each of these cells a new FTO/TiO_2/Cu_2S was prepared to account for some unavoidable variations in the conditions and geometry of the photocatalytic deposition of copper nanoparticles on the titania surface and the following procedure of transformation of copper into Cu_2S.

The data presented in Table 2 shows that the PEC parameters of the CIS@ZnS-based cells are quite satisfactorily reproducible, the values of J_{sc}, V_{oc}, and FF varying from the averaged values by around 5%. As the η value is a combination of these parameters ($\eta = J_{sc} \times V_{oc} \times FF \times I^{-1}$, where I is the light intensity in mW cm^{-2}), the uncertainties of J_{sc} and FF determination "mute" each other and the total light conversion efficiency of the six studied cells deviates from the average value, 8.15%, by a mere one percent. It can be concluded therefore that the solar cells studied in the present paper reveal very good reproducibility of the photoelectrochemical parameters. This reproducibility is accompanied by the robustness of the cells that keep unchanged their PEC parameters after a week trial with intermittent illumination and for more than two hours of continuous illumination.

The data presented in Table 2 also shows explicitly that the deposition of a ZnS shell has a very pronounced effect on the PEC efficiency of CIS NPs increasing the total light conversion efficiency from 5.7% in average for CIS- to 8.15% for CIS@ZnS-based cells, that is by 43%. A similar effect of a wider-bandgap shell was previously observed for the CIS-based liquid-junction cells[7,22] and associated with the elimination of non-radiative recombination sites on the CIS NP surface by a ZnS shell which is in accordance with the PL data discussed earlier in the present paper.

The open-circuit voltage of around 0.6 V is typical for the CIS-based liquid-junction solar cells.[11] The V_{oc} is roughly the same for CIS- and CIS@ZnS-based photoanodes indicating that the thin ZnS shell deposition does not alter appreciably the energy levels alignment on the interfaces between CIS, TiO_2 and polysulfide electrolyte. The ZnS passivating layer is often reported to suppress the recombination of the charge carriers photogenerated in CIS(Se) NPS and the electrolyte species, the ZnS shell deposition typically results in an increase in V_{oc}.[11,46,47] In the present case, the ZnS shell deposition enhances the photocurrent and PL intensity but does not alter V_{oc}, the facts summarily indicating that the shell influences the photoanode efficiency rather by passivating the CIS NP surface states and by suppressing the radiationless electron–hole recombination within the CIS NPs.

The fill factor values are seemingly low as compared, for example, to the dye-sensitized solar cells based on the nanocrystalline titania.[48] However, a comparison of the presented values with those reported for similar systems shows that these are quite typical parameters. For example, the FF of only 31–32% was reported by S. J. Rosenthal *et al.* for a liquid-junction solar cell based on plasmonic CIS NPs and aqueous polysulfide electrolyte.[21] Probably the highest FF of 0.58 was reported in ref. 11 for the liquid-junction solar cell based on a TiO_2/CIS@ZnS photoanode, polysulfide electrolyte, and Cu_xS-based counter-electrode. However, by the total light-to-current conversion efficiency the cells reported here supersede typical values reported for ternary chalcopyrite-based liquid-junction solar cells. For example, for the above-mentioned cells comprising plasmonic CIS NPs the average efficiency of 3.1% was reported in ref. 21, while the top η of 6.6% was reported in ref. 11 for the similar cell however produced by a more complex method.

Conclusion

We have reported a direct "green" aqueous synthesis of mercapto acetate-stabilized copper indium sulfide NPs of a varied composition that can be easily deposited onto the surface of nanocrystalline FTO/TiO_2 films without any preliminary purification yielding the visible-light-sensitive photoanodes for the liquid-junction solar cells. The proposed approach enables the fast and easy formation of the TiO_2/CIS@ZnS heterostructures at ambient conditions avoiding the steps of phase transfer, NPs precipitation, ligand exchange, dialysis, *etc.* used in alternative approaches for producing similar composites.[23]

Systematic variation of the NP composition, that is the content of copper, indium and sulfur, as well as the amount of ZnS deposited as a protective shell on the surface of CIS NPs

showed that the highest photoelectrochemical activity was demonstrated by a TiO_2/CIS@ZnS photoanode with a molar Cu : In : S ratio of 1 : 5 : 10 and a ZnS shell produced as a molar Zn : Cu ratio of 1 : 1.

It was found also that the photoelectrochemical activity of TiO_2/CIS@ZnS heterostructures and the PL intensity of original colloidal CIS@ZnS NPs change in a similar manner at the variations of copper and indium content allowing to use PL as an indicative parameter when designing CIS-based absorbers for the PEC solar cells.

The TiO_2/CIS@ZnS heterostructures with the optimal composition were studied by a combination of X-ray photoelectron, Raman, and energy-dispersive X-ray spectroscopy, X-ray diffraction and scanning electron microscopy to gain insight into the morphology and composition of such photoanodes. The Raman spectra of CIS NPs revealed a set of features typical for stoichiometric and copper-poorer chalcopyrite phases that are preserved after the ZnS shell formation and deposition of the CIS@ZnS NPs onto the titania surface. The XPS confirmed the copper and indium present as Cu(I) and In(III) and successful formation of a ZnS shell in the case of CIS@ZnS NPs. The atomic Cu : In ratio both in the original CIS NPs and the CIS@ZnS NPs deposited onto the surface of TiO_2 is close to 1 : 5, as anticipated by the synthetic procedure.

The optimized TiO_2/CIS@ZnS photoanodes with Cu : In : S and Zn : Cu ratios of 1 : 5 : 10 and 1 : 1 were tested in two-electrode solar cells with aqueous polysulfide electrolyte and TiO_2/Cu_2S heterostructures produced by a photo-assisted method as counter-electrodes. The cells revealed good stability providing steady PEC parameters during more than 2 h continuous illumination and at least a week period of intermittent illumination as well as reproducibility of the light conversion efficiency. Under solar-like illumination with an intensity of 30 mW cm^{-2}, the optimized cells showed the average light conversion efficiency of 8.15% with the average open-circuit voltage close to 0.6 V and the average fill factor of 0.42. Similar solar cells based on CIS NPs that were not covered with a ZnS shell demonstrated a far inferior activity with the light conversion efficiency around 5.75% indicating a crucial role of the passivation of surface defects of CIS NPs for achieving the efficient charge collection from the TiO_2/CIS photoanodes.

Acknowledgements

The work was supported by Volkswagen Foundation (project "New functionalities of semiconductor nanocrystals by controllable coupling to molecules"). Authors acknowledge the help of N. Skorik and V. Moskalyuk (LLC Nanomedtech, Kyiv, Ukraine) with acquiring the SEM and EDX data and Dr S. Schulze (TU Chemnitz) for TEM measurements. The clipart used in Scheme 1 was freely downloaded from http://www.openclipart.com.

References

1 *Semiconductor nanocrystal quantum dots: synthesis, assembly, spectroscopy and applications*, ed. A. Rogach, Springer-Verlag GmbH, Vienna, 2008, p. 372.
2 D. V. Talapin, J.-S. Lee, M. V. Kovalenko and E. V. Shevchenko, *Chem. Rev.*, 2010, **110**, 389.
3 I. J. Kramer and E. H. Sargent, *ACS Nano*, 2011, **5**, 8506.
4 P. V. Kamat, *J. Phys. Chem. Lett.*, 2013, **4**, 908.
5 H. Zhong, Z. Bai and B. Zou, *J. Phys. Chem. Lett.*, 2012, **3**, 3167.
6 S. Liu and X. Su, *RSC Adv.*, 2014, **4**, 43415.
7 A. D. P. Leach and J. E. Macdonald, *J. Phys. Chem. Lett.*, 2016, **7**, 572.
8 J. Kolny-Olesyak and H. Weller, *ACS Appl. Mater. Interfaces*, 2013, **5**, 12221.
9 Y. Tang, P. Wang, J.-H. Yun, R. Amal and Y. H. Ng, *J. Mater. Chem. A*, 2015, **3**, 15876.
10 S. Wang, X. Yang, Y. Zhu, Y. Su and C. Li, *RSC Adv.*, 2014, **4**, 23790.
11 Z. Pan, I. Mora-Sero, Q. Shen, H. Zhang, Y. Li, K. Zhao, J. Wang, X. Zhong and J. Bisquert, *J. Am. Chem. Soc.*, 2014, **136**, 9203.
12 B. Chen, S. Chang, D. Li, L. Chen, Y. Wang, T. Chen, B. Zou, H. Zhong and A. L. Rogach, *Chem. Mater.*, 2015, **27**, 5949.
13 M. Gannouni, I. Ben Assaker and R. Chtourou, *Int. J. Hydrogen Energy*, 2015, **40**, 7252.
14 P. V. Kamat, *J. Phys. Chem. C*, 2008, **112**, 18737.
15 W. Yue, M. Wang and G. Nie, *Sol. Energy*, 2014, **99**, 126.
16 H. Fakhri, A. R. Mahjoub and A. H. Cheshme Khavar, *Appl. Surf. Sci.*, 2014, **318**, 65.
17 W. Bo, Z. Liu, T. Hong, J. Han, K. Guo, X. Zhang and D. Chen, *J. Nanopart. Res.*, 2015, **17**, 295.
18 P. Niyamakom, A. Quintilla, K. Köhler, M. Cemernjak, E. Ahlswede and S. Roggan, *J. Mater. Chem. A*, 2015, **3**, 4470.
19 M. Hong, T. Xuan, J. Liu, Z. Jiang, Y. Chen, X. Chen and H. Li, *RSC Adv.*, 2015, **5**, 102682.
20 T. Omata, K. Nose, K. Kurimoto and M. Kita, *J. Mater. Chem. C*, 2014, **2**, 6867.
21 J. Scott Niezgoda, E. Yap, J. D. Keene, J. R. McBride and S. J. Rosenthal, *Nano Lett.*, 2014, **14**, 3262.
22 M. Sun, D. Zhu, W. Ji, P. Jing, X. Wang, W. Xiang and J. Zhao, *ACS App. Mater. Interfaces*, 2013, **5**, 12681.
23 R. Wang, Y. Shang, P. Kanjaboos, W. Zhou, Z. Ning and E. H. Sargent, *Energy Environ. Sci.*, 2016, **9**, 1130.
24 H. Zhong, Z. Bai and C. Zou, *J. Phys. Chem. Lett.*, 2012, **3**, 3167.
25 B. Zhang, Y. Wang, C. Yang, S. Hu, Y. Gao, Y. Zhang, Y. Wang, H. V. Demir, L. Liu and K.-T. Yong, *Phys. Chem. Chem. Phys.*, 2015, **17**, 25133.
26 J. Zhang, W. Sun, L. Yin, X. Miao and D. Zhang, *J. Mater. Chem. C*, 2014, **2**, 4812.
27 Y. Chen, S. Li, L. Huang and D. Pan, *Nanoscale*, 2014, **6**, 1295.
28 W.-H. Zhou, J. Jiao, Y. Zhao, X.-Y. Cheng, D.-X. Kou, Z.-J. Zhou and S.-X. Wu, *RSC Adv.*, 2014, **4**, 7617.
29 C. Sun, Z. Cevher, J. Zhang, B. Gao, K. Shum and Y. Ren, *J. Mater. Chem. A*, 2014, **2**, 10629.
30 A. V. Kozytskiy, O. L. Stroyuk, M. Skoryk and S. Y. Kuchmiy, *Photochem. Photobiol. Sci.*, 2015, **14**, 942.
31 A. V. Kozytskiy, O. L. Stroyuk and S. Y. Kuchmiy, *Theor. Exp. Chem.*, 2015, **51**, 203.

32 D. H. Jara, K. G. Stamplecoskie and P. V. Kamat, *J. Phys. Chem. Lett.*, 2016, **7**, 1452.
33 G. Zaiats, S. Kinge and P. V. Kamat, *J. Phys. Chem. C*, 2016, **7**, 1452.
34 J. F. Moulder, W. F. Stickle, P. E. Sobol and K. D. Bomben, *Handbook of X Ray Photoelectron Spectroscopy: A Reference Book of Standard Spectra for Identification and Interpretation of Xps Data*, Physical Electronics, 1995.
35 A. V. Naumkin, A. Kraut-Vass and S. W. Gaarenstroom, *NIST X-ray Photoelectron Spectroscopy Database, NIST, Stand. Ref. Database 20, Version 4.1*, 2012.
36 J. Lee and C.-S. Han, *Nanoscale Res. Lett.*, 2015, **10**, 145.
37 W. Meng, X. Zhou, Z. Qiu, C. Liu, J. Chen, W. Yue, M. Wang and H. Bi, *Carbon*, 2016, **96**, 532.
38 A. Fairbrother, V. Izquierdo-Roca, X. Fontané, M. Ibáñez, A. Cabot, E. Saucedo and A. Perez-Rodriguez, *CrystEngComm*, 2014, **16**, 4120.
39 M. Dimitrievska, A. Fairbrother, X. Fontané, T. Jawhari, V. Izquierdo-Roca, E. Saucedo and A. Perez-Rodriguez, *Appl. Phys. Lett.*, 2014, **104**, 021901.
40 J. Li, B. Kempken, V. Dzhagan, D. R. T. Zahn, J. Grzelak, S. Mackowski, J. Parisi and J. Kolny-Olesiak, *CrystEngComm*, 2015, **17**, 5634.
41 B. Kempken, V. Dzhagan, D. Zahn, M. J. P. Alcocer, I. Kriegel, F. Scotognella, J. Parisi and J. Kolny-Olesiak, *RSC Adv.*, 2015, **5**, 89577.
42 V. Izquierdo-Roca, A. Shavel, E. Saucedo, S. Jaime-Ferrer, J. Álvarez-García, A. Cabot, A. Perez-Rodriguez, V. Bermudez and J. R. Morante, *Sol. Energy Mater. Sol. Cells*, 2011, **95**, S83.
43 V. M. Dzhagan, A. P. Litvinchuk, M. Y. Valakh, M. Kruszynska, J. Kolny-Olesiak, C. Himcinschi and D. R. T. Zahn, *Phys. Status Solidi*, 2014, **211**, 195.
44 N. M. Gasanly, S. A. El-Hamid, L. G. Gasanova and A. Z. Magomedov, *Phys. Status Solidi*, 1992, **169**, K115.
45 B. Chen, H. Zhong, W. Zhang, Z. Tan, Y. Li, C. Yu, T. Zhai, Y. Bando, S. Yang and B. Zou, *Adv. Funct. Mater.*, 2012, **22**, 2081.
46 J.-Y. Kim, J. Yang, J. H. Yu, W. Baek, C.-H. Lee, H. J. Son, T. Hyeon and M. J. Ko, *ACS Nano*, 2015, **9**, 11286.
47 J.-Y. Chang, C.-H. Li, Y.-H. Chiang, C.-H. Chen and P.-N. Li, *ACS Appl. Mater. Interfaces*, 2016, **8**, 18878.
48 M. Grätzel, *J. Photochem. Photobiol., C*, 2003, **4**, 145.